Pergamon

Journal of Structural Geology, Vol. 17, No. 12, pp. 1637 to 1654, 1995
Elsevier Science Ltd
Printed in Great Britain
0191-8141/95 $9.50+0.00

0191-8141(95)00068-2

Thrust kinematics and transposition fabrics from a basal detachment zone, eastern Australia

DAVID R. GRAY

Australian Geodynamics Cooperative Research Centre, Department of Earth Sciences, Monash University, Melbourne, Victoria 3168, Australia

(*Received* 2 *September* 1994; *accepted in revised form* 22 *May* 1995)

Abstract—Emplacement of an upper crustal, leading imbricate-fan thrust belt in the Lachlan Fold Belt of eastern Australia was accomplished along a 0.5–1 km thick zone of heterogeneously deformed, low grade phyllonite in pelitic rock. Continuous recrystallization and neocrystallization of mica in a zone of transposition layering has provided a weak zone at the base of a 100 km wide × 150 km exposed length × 10 km thick thrust system. The basal deformation zone is characterized by a low–moderately dipping, strong–intense transposition foliation enclosing elongate fault-bounded slices (up to 20 km long × 5 km wide in map view) of disrupted Cambrian metavolcanics and Upper Ordovician black shales and slates. These are derived from a structurally lower zone of duplexing or from the overturned limbs of anticlinorial structures. The detachment zone is a 10–15 km wide zone of intense deformation showing a transition from open, upright folds with weak cleavage to inclined, tight–isoclinal folds with strong axial surface cleavage. The intensity of minor faults also increases into the zone. Leading imbricate fan thrust belts show maximum deformation effects along the basal detachment which forms the frontal or leading fault. The leading imbricate geometry is due to emplacement of the basal detachment zone up the lowest and last formed imbricate thrust. Movement is along a relatively ductile, low viscosity 'layer' at the base where strain softening occurs with development of transposition layering. This enables confined 'flow' along the basal zone with transport and emplacement of the fold system and duplex zone to higher structural levels. Reaction-enhanced ductility and grain boundary sliding may be important deformation mechanisms responsible for this flow. Localized polydeformation, marked by mesofolds and crenulation cleavage, reflects the interaction between thrust sheets and the movement on faults.

INTRODUCTION

Exposed detachment zones provide direct information about the processes involved in transport and emplacement of thrust sheets to higher crustal levels. The nature of fabrics, folds, strain states and incremental strain histories within these basal deformation zones are a direct consequence of the thrusting and emplacement mechanisms (e.g. Elliott 1976). Systematic strain variations within thrust sheet volumes reflect their mode of emplacement (e.g. Sanderson 1982, Fischer & Coward 1982, Geiser 1988, Mitra 1994). Relationships between structures higher within thrust sheets relative to structures within detachment zones can provide contrasting information about thrust-sheet emplacement. Complexity can result from the superposition of structures formed during detachment, motion of the sheet and emplacement to higher crustal levels.

This paper investigates the structural transition from a simply folded belt into a major detachment zone associated with E-vergent thrusting in the Lachlan Fold Belt of eastern Australia (Fig. 1). The geometry of the fault zone is established through maps and structural profiles based on detailed work from generally weathered exposures limited to road cuttings, creeks and rivers; straddling the Great Dividing Range of eastern Australia the region is rugged, thickly vegetated and mountainous by Australian standards, with elevations up to 1500 m and access commonly by four-wheel drive (4WD) tracks. The kinematic evolution of the fault zone has been inferred from total and incremental strain data and sequences of crenulation cleavages. The work concentrates on field and laboratory observations of the structures and deformation mechanisms within the detachment zone, with particular relevance to thrust motion and emplacement mechanisms at low greenschist facies conditions. The paper documents structures, geometry and kinematics for a leading imbricate fan thrust belt and looks at the consequences for development of this type of thrust system.

GEOLOGICAL SETTING

The western Lachlan Fold Belt (Fig. 1) is made up of a deformed turbidite sequence cut by a series of major west-dipping, reverse faults which link to a mid-crustal detachment fault (e.g. Gray & Willman 1991a,b, Gray *et al.* 1991, Glen 1992, Fergusson & Coney 1992). Part of an E-vergent fold and thrust belt, the reverse faults expose Cambrian mafic volcanics, cherts and volcaniclastics in their immediate hanging walls. Thrust sheets largely consist of chevron-folded sandstone and mudstone layers which reflect up to 65% shortening above this mid-crustal detachment fault (Gray & Willman 1991a). Deep crustal seismic profiling (Gray *et al.* 1991) and microseismicity studies (Gibson *et al.* 1981) require this detachment to be at approximately 15–17 km depth. The detachment fault shallows to the east into the Melbourne Zone where it is exposed as the Mount Wellington Fault Zone (Fergusson *et al.* 1986, Murphy

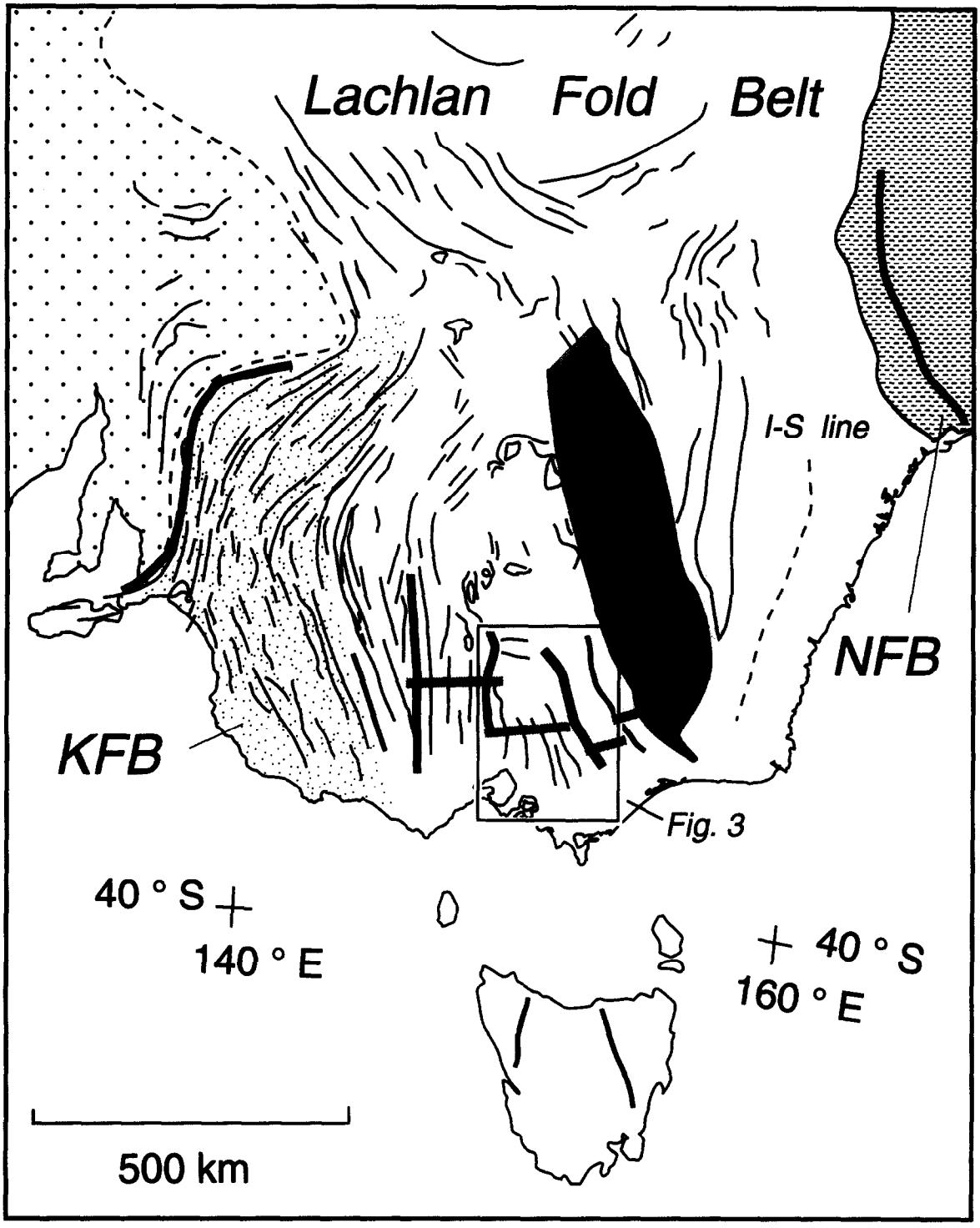

Fig. 1. Structural trend map of the Palaeozoic Tasman Orogenic Belt of southeastern Australia, combining aeromagnetic trend lines and outcrop traces from both regional maps and satellite images. Two-thirds of the area shown is hidden by cover sequences of younger sedimentary basins. Faults: heavy lines; light stipple: Early Palaeozoic Kanmantoo Fold Belt (KFB); dashes: Late Palaeozoic New England Fold Belt (NFB); shading: Wagga–Omeo Metamorphic Belt (WMB); dashed line: cratonic line demarcating Proterozoic (coarse stipple) from Palaeozoic crustal rocks to the east. Position of regional section line (Fig. 2) and regional map (Fig. 3) are shown.

& Gray 1992; see Fig. 2). This fault zone is a major upper crustal discontinuity that separates fold–thrust zones of different age and vergence (Fig. 2). In the western Lachlan Fold Belt (Stawell, Ballarat–Bendigo and Melbourne Zones; Fig. 2) structures are E-vergent and are related to a post-Silurian deformation event, whereas those to the east (Tabberabbera Zone; Fig. 2) show vergence to the southwest and are related to a Late Ordovician/Early Silurian deformation event (Gray 1988).

FAULT ZONE CHARACTER

The Mount Wellington Fault Zone (Fig. 2) is a 20 km thick, northwest striking zone of intense deformation

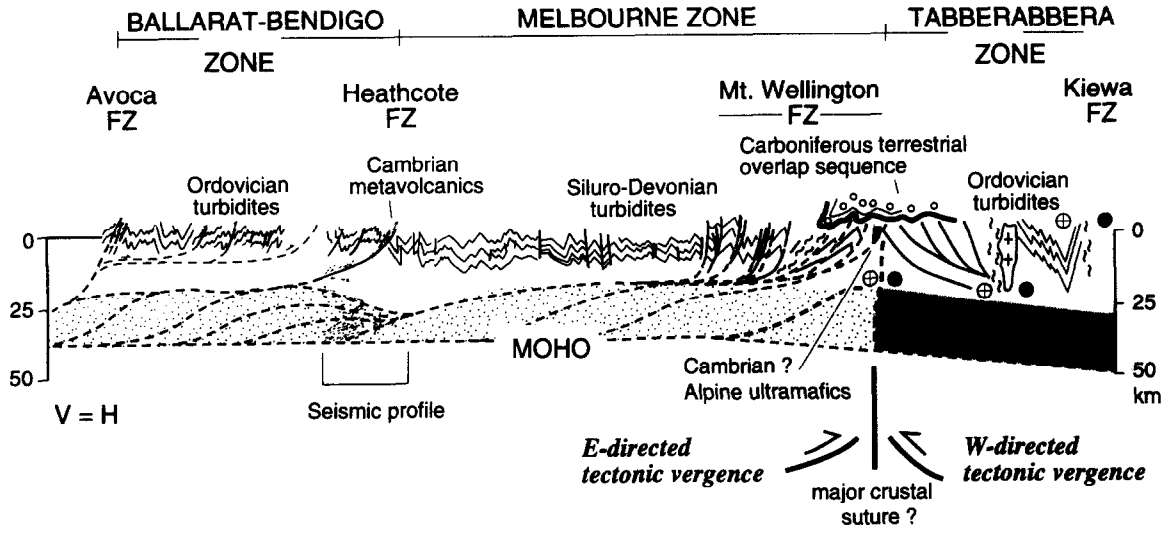

Fig. 2. Regional structural profile showing inferred relationships of the upper crustal structure to that of the lower crust (modified from Gray *et al.* 1991).

along the eastern margin of the Melbourne Zone (includes structural zones 3 and 4: Fig. 3). It has a map length of 100 km and a map width of 30 km, but is covered to the north by sediments of the Murray Basin and to the south by Cretaceous–Tertiary sediments of the Gippsland Basin. Most of the Mount Wellington Fault Zone consists of a strongly deformed, undifferentiated Lower Palaeozoic succession of unfossiliferous quartz turbidite beds and mudstone, containing many elongate fault slivers (possibly horses) of Cambrian, Ordovician and Silurian rocks (Harris & Thomas 1954, VandenBerg 1978). The oldest rocks in this belt are Cambrian mafic volcanic rocks, volcaniclastic rocks, shale, limestone and chert. The Ordovician rocks in the Mount Wellington Fault Zone are Early Ordovician quartz-rich turbidites and cherts, and Late Ordovician black shales.

Four main structural zones (Table 1) characterize the structural style and geometry from simply folded rocks of the upper part of the composite thrust system into the more intensely deformed rocks of the Mount Wellington Fault Zone (Figs. 3 and 4). Folds outside the influence of the fault zone (zone 1: Fig. 3) tend to be upright, open to tight chevron folds cut by steeply dipping reverse faults (zone 1: Fig. 4). Major anticlinoria and synclinoria are spaced at approximately 20 km intervals and have wavelengths of ~40 km and amplitudes of ~4 km. Regionally, fold interlimb angles range from 70 to 100° with folds either showing a weak reticulate or no cleavage fissility at all (zone 1, Fig. 4). Fold shortening in this zone is ~25%. Where cleavage is more strongly developed (zone 2: Fig. 4) there is a transition from more open folds with interlimb angles between 55 and 70° (zone 2a) to tighter folds with interlimb angles generally between 30 and 50° (zone 2b). Fold shortening is ~53% (zone 2a)–64% (zone 2b). Where cleavage is intense and folds are inclined and cut by significant numbers of faults (zone 3: Fig. 4), the fold interlimb angles generally range between 20 and 30°, but may contain folds with interlimb angles of 50°. Fold shortening in this zone is at least 65%. Within the most strongly deformed part of the fault zone (zone 4: Figs. 3 and 4) narrow, elongate (up to 20 km in strike length and 4 km outcrop width) fault slivers of different ages occur within strongly foliated phyllonite (Fig. 5).

Accompanying this west–east fold tightening and increasing development of cleavage to intense foliation across the Melbourne Zone is a transition from upright folds (Figs. 6a&b and 7b) to inclined and overturned folds (Figs. 6c–e and 7a). Within the Mount Wellington Fault Zone (zone 3: Fig. 4) the regional F_1 folds are asymmetric, tight to isoclinal, northeast verging folds with an axial planar S_1 slaty cleavage (Fig. 7a). They are cut by W-dipping faults and shear zones with localized multiple deformation (Figs. 6c&e and 7d–f).

Fault Slices

Fault-bounded slices of Upper Ordovician black mudstone/slate and Cambrian metavolcanic rocks have tapered ends, are elongated sub-parallel to the regional strike of the fault zone and show variations in younging, vergence, amount of strain and degree of metamorphism. The Ordovician slices occur west of the Cambrian slices (Fig. 5) and are therefore structurally higher. Some occur as isolated slices within the turbidites or are in fault contact with the mafic volcanics. Most tend to have moderately SW-dipping cleavage and steeply SW-dipping bedding with vergence to the southwest, indicating derivation from the overturned eastern limbs of the regional asymmetric F_1 anticlines. The bounding faults are aligned sub-parallel to the regional foliation and tend to dip moderately–steeply southwest (Fig. 6e).

The Cambrian inliers have complex internal stratigraphy truncated by bounding faults, and are offset by N- and NE-trending cross-faults. The largest inliers consist of an internally faulted sequence of andesitic lavas, agglomerates, mafic boninites, pillowed and massive tholeiitic basalts, and gabbroic–doleritic intrusives (Crawford 1988). Sequences within the Cambrian inliers

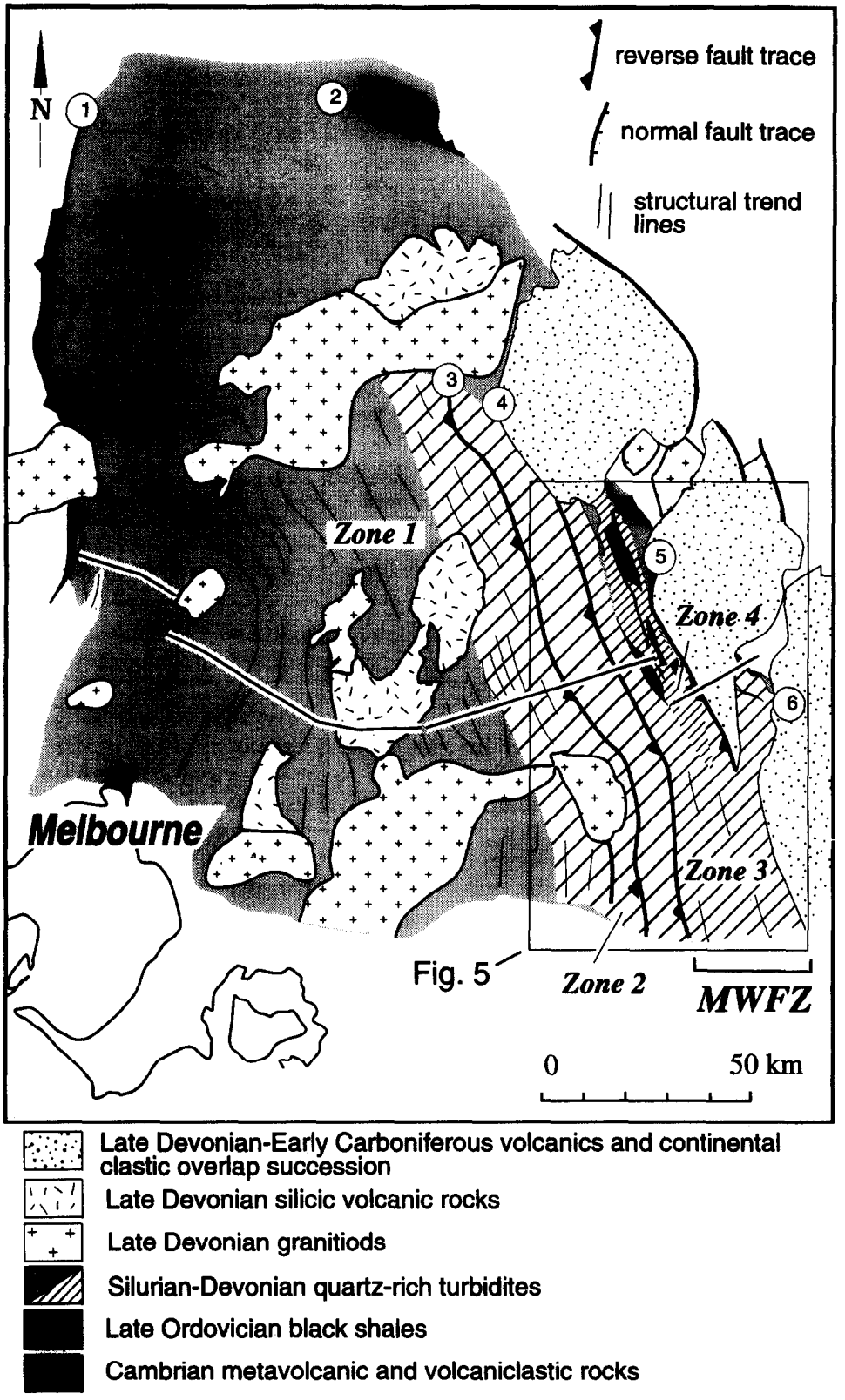

Fig. 3. Structural trend map of the Melbourne Zone, showing outcrop traces of major faults, fold axial surface traces, granite intrusives and trend lines. The locations of Fig. 5 and the cross-section in Fig. 4 are shown. Major faults are designated by the circled numbers: (1) Heathcote Fault Zone; (2) Dookie Thrust; (3) Enochs Point Thrust; (4) Mansfield Thrust; (5) Barkly Thrust; (6) Dolodrook Fault Zone; MWFZ: Mount Wellington Fault Zone.

vary from moderate–steeply NE-dipping with pillow basalts indicating NE younging (Howqua inlier, Fig. 5) to moderate SW-dipping and younging (Jamieson inlier, Fig. 5). Within the Jamieson inlier (Fig. 5), contacts between units are strongly foliated shear zones up to 100 m wide showing augen structures and *S–C* fabrics with a top to the east sense (Hendrickx 1993). All of the inliers have largely undeformed cores which preserve the original igneous textures, stratigraphy and mineralogy of burial metamorphism (prehnite–pumpellyite and

Table 1. Structural zonation across the Melbourne Zone into the Mount Wellington Fault Zone

West			East
Zone 1	Zone 2	Zone 3	Zone 4
Open, upright folds	2a: Open, upright folds 2b: Close, upright folds	Close–tight, inclined folds	Tight–isoclinal, inclined folds cut by numerous faults
70–100° ILA*	2a: 55–70° ILA 2b: 30–50° ILA	20–50° ILA	
25% Fold shortening	2a: 53% Fold shortening 2b: 64% Fold shortening	~65% Fold shortening	>70% Shortening
Weak reticulate cleavage, pencil structure, or no cleavage	2a: Pencil structure/weak cleavage 2b: Moderate–strong cleavage	Strong cleavage	Strong cleavage–intense foliation in shear zones
Anchizone (sub-greenschist facies) (0.25–0.30 IC†)	2a: Anchizone (sub-greenschist facies) (0.25–0.30 IC) 2b: epizone (greenschist facies) (0.23–0.25 IC)	Greenschist facies (<0.20 IC)	Greenschist facies (<0.20 IC)
Faults minor Steep reverse faults with both east and west dip	Steep reverse faults with both east and west dip	Steep–moderately W-dipping reverse faults	Numerous, low angle, W-dipping reverse/thrust faults and shear zones, containing horses of Upper Ordovician shale and Cambrian meta-volcanics, limestones and volcaniclastics

*ILA: fold interlimb angle (ILA values measured off regional profile, but ILA does vary locally at the outcrop scale).
†IC: illite crystallinity values (Robin Offler personal communication).

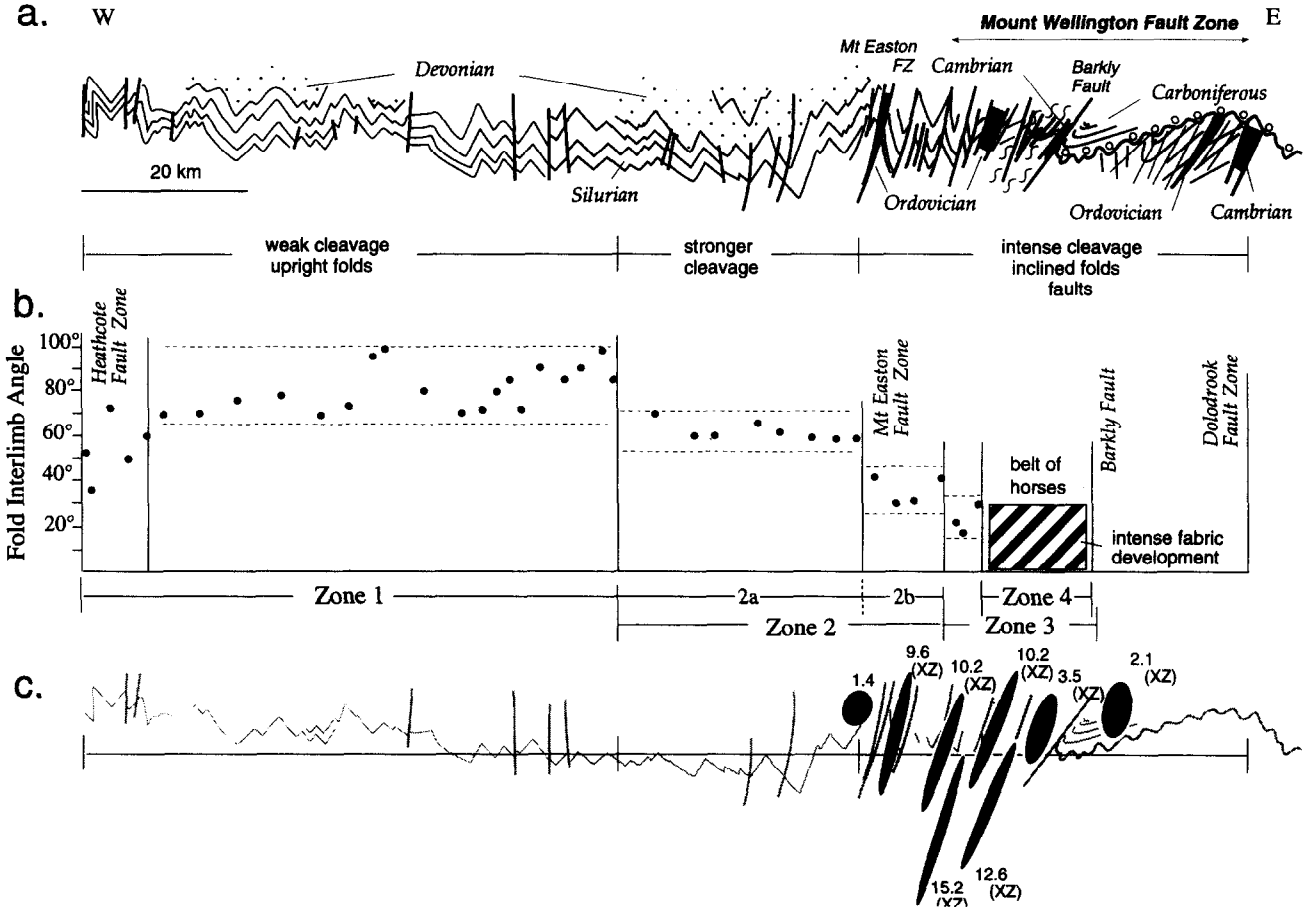

Fig. 4. Regional structural profile (a) for the Melbourne Zone showing increase in strain from west to east into the Mount Wellington Fault Zone (see Fig. 3 for location) (modified from VandenBerg 1988, fig. 4.1). (b) Plot of regional fold interlimb angle vs position on the profile in (a). The four structural zones have distinct fold tightness. (c) Total X/Z strain data plotted as black ellipses on the regional structural profile in (a).

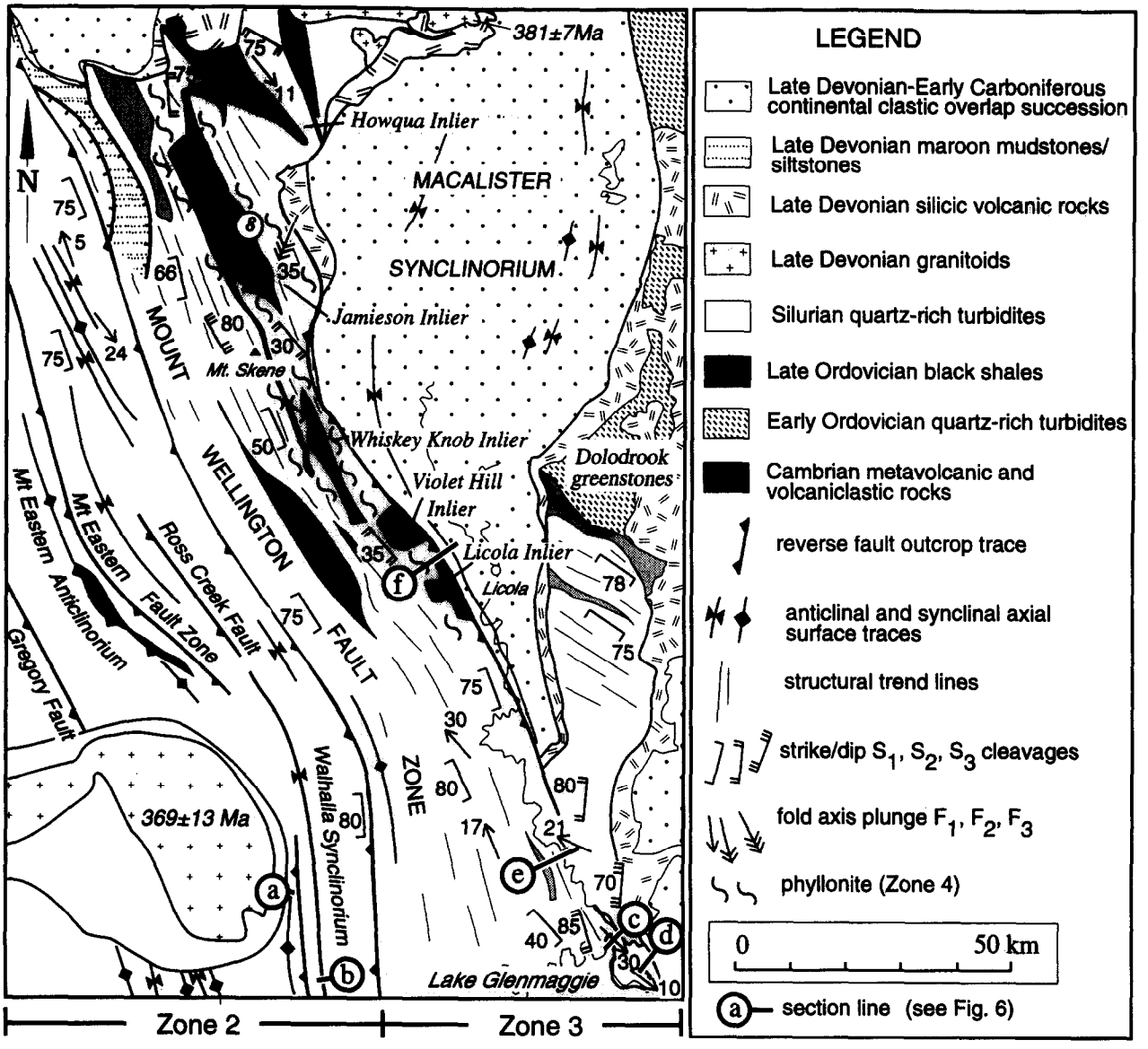

Fig. 5. Geological map of the Mount Wellington Fault Zone, showing the main structural elements of the fault zone, the Cambrian mafic volcanic inliers and the fault-bounded slices of Ordovician black shale and the overlying cover sequences of the Macalister and Avon Synclinoria. (Geology modified from Warburton 1:250,000 Map Sheet; VandenBerg 1977). The position of section lines a–e (see Fig. 6) and f (see Fig. 10) and the structural zones are shown.

prehnite–actinolite facies; Crawford 1988, Hendrickx 1993). Towards the margins of the inliers, the metavolcanic rocks show increasing effects of deformation with development of a strong foliation defined by chlorite, tremolite/actinolite fibres and granular epidote (metabasalts). Bounding faults tend to be N–NW-trending, brittle zones of silicification and brecciation up to 30 m wide.

Polydeformed zones

Polydeformed zones occur as fault-bounded, approximately strike-parallel high strain zones within the sequence (Figs. 6c&d) and are characterized by interfering mesofolds and overprinting crenulation cleavages (see Murphy & Gray 1992). The F_1 folds within these zones show varying geometry and departures from the regional fold axis orientation. The F_1 fold axes appear to swing from NNW- to E-trending and change from inclined plunging folds (Figs. 6c&d) to recumbent folds (Fig. 6c: polydeformed zone) with reclined geometry where overprinting F_2 and F_3 produce complex refolding relationships and localized development of S_2 and S_3 cleavages. In these polydeformed zones where $S_2 \wedge S_3 < 30°$, D_3 structures reorient the D_2 structures rather than producing F_3 fold interference structures (cf Odonne & Vialon 1987).

KINEMATICS OF THRUSTING

Total strain states, incremental strain histories from fibres in pressure shadows, overprinting crenulation cleavages, as well as the fabric and microstructure of the transposition layering, provide information about the mechanisms and kinematics of thrusting. Each of these will now be discussed.

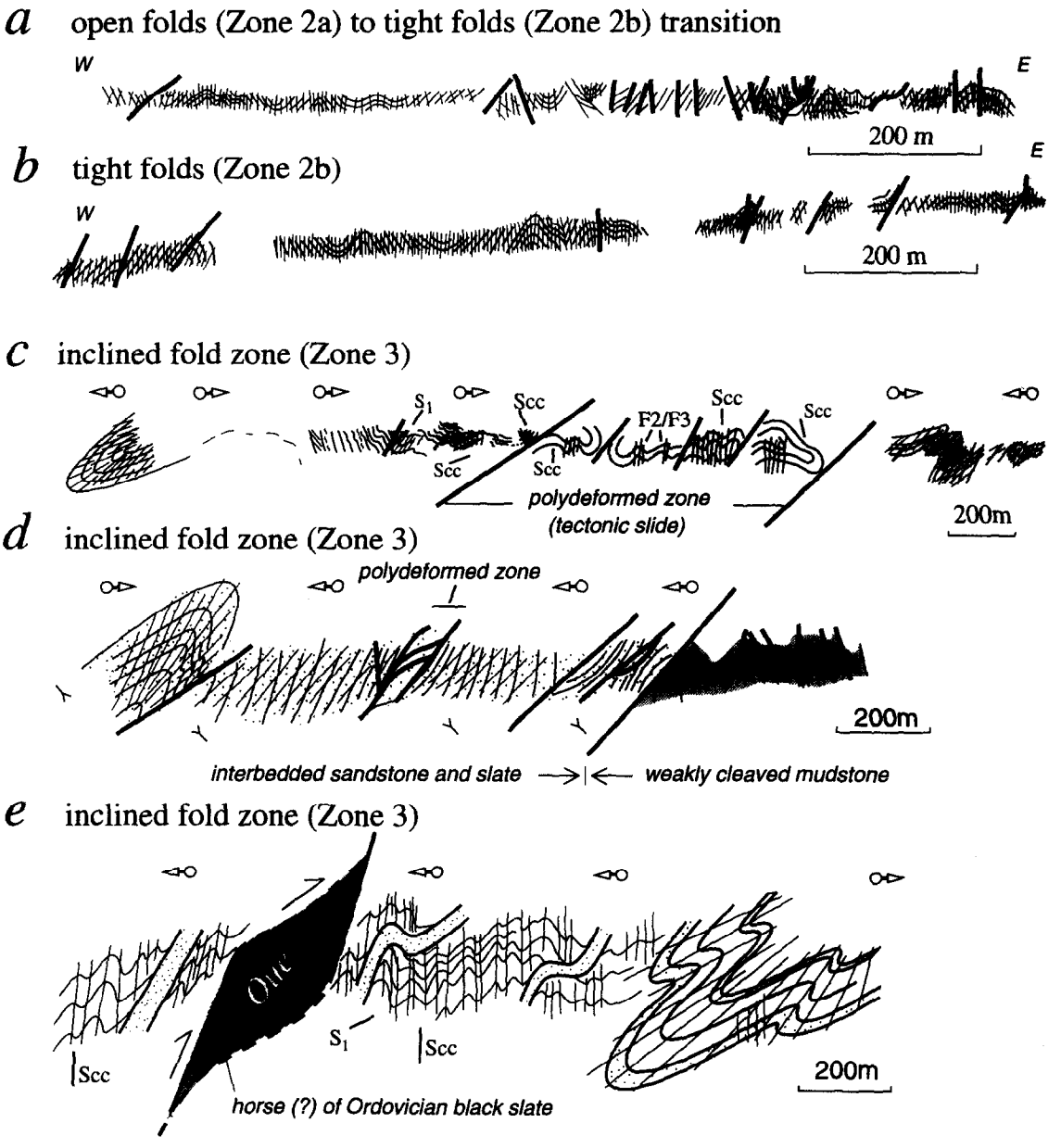

Fig. 6. Structural profiles showing shape, tightness and geometry of folds across the different structural zones into the Mount Wellington Fault Zone; open folds with weak cleavage of zone 2 (section a), tight folds with moderate cleavage of zone 2 (sections a and b) and inclined to overturned folds of zone 3 (sections c–e). For locations, see Fig. 5. (Sections c and d are modified from Murphy & Gray 1992.)

Total strain states

The main part of the fault zone (zone 4: Fig. 5) is dominated by a moderately SW-dipping foliation. The magnitude (Table 2) and orientation of the total strain ellipsoid relative to this foliation (see Fig. 3c) have been determined from the following structural elements.

(1) Deformed cooling columns (Fig. 7c) within porphyritic andesite lava flows by treating the segments which make up the individual polygonal form (viewed in sections perpendicular to the column long axes) as a series of initially random line segments (cf Sanderson 1977). Strain states (X/Z) range from 2.0:1 (Licola inlier) to 3.5:1 (Jamieson inlier) (see Table 2 and Appendix).

(2) Quartz fibre pressure shadows on pyrite in lineated biotite–pyrophyllite rhyolitic rocks within the Jamieson inlier, by the Pyrite method (cf Durney & Ramsay 1973, p. 92). The total X/Z strain state was 12.6:1 (see Table 2 and Appendix).

(3) Quartz fibre pressure shadows on pyrite (Fig. 8h) in Upper Ordovician black mudstone/slate horses, by comparing the relative length of the fibres to the radius of the host pyrite (cf Durney & Ramsay 1973, Spencer 1991). Total X/Z strain states range from 9.0:1 to 18.4:1 (Jamieson slice) (see Table 2 and Appendix).

(4) Quartz fibre pressure shadows on pyrite (Fig. 7i) in mudstone layers within the folded sandstone, siltstone, mudstone turbidite sequence (undifferentiated Palaeozoic rocks), by comparing the relative length of the fibres to the radius of the host pyrite (cf Durney & Ramsay 1973, Spencer 1991). Total X/Z strain states range from 6.3:1 to 15.2:1 (see Table 2 and Appendix).

In each case the maximum principal stretch direction

X is sub-parallel to the dip-direction of the foliation and the foliation approximates the XY plane of the total strain ellipsoid. Strain magnitude clearly increases from the upright fold zone (zone 2; X/Z strains < 6.3:1) into the inclined fold zone (zone 3; X/Z strains between 9.6:1 and 15.2:1) (see Figs. 3c and 9) and matches the increase in cleavage intensity into the Mount Wellington Fault Zone. The magnitude of total strain varies within the Cambrian mafic volcanic inliers, with less deformed cores giving X/Z strains < 3.5:1 and the more strongly deformed, foliated parts with X/Z = 12.6:1.

Incremental strain histories

The shapes and curvature of quartz fibres in pressure fringes on pyrite within some of the mudstones record the incremental extension history during foliation development (e.g. Durney & Ramsay 1973, Gray & Durney 1979). Fibre geometries in rare pressure fringes from mudstones within the Mount Wellington Fault Zone are generally straight indicating a co-axial deformation sequence for upright limbs and hinges of the asymmetric regional folds (see Table 1). All samples located have been from less deformed segments where bedding and cleavage is part of the inclined to overturned regional folding (zone 3: Fig. 5). Unlike the Ballarat Slate Belt of central Victoria (cf Gray & Willman 1991a), pressure fringes are uncommon within mudstones of the Mount Wellington Fault Zone due to a lower pyrite content.

Some samples show two cleavages (slaty cleavage S_1 and a superimposed crenulation cleavage S_2 or S_3). In one case, the fibre geometry of an accompanying pressure shadow shows a pronounced curvature where the two largely straight fibre segments are aligned sub-parallel to S_1 and the respective crenulation cleavage (see Fig. 8j). This reflects a continuous rather than episodic deformation sequence with rapid changes in the incremental extension direction associated with localized development of crenulation cleavages (e.g. Gray & Durney 1979, fig. 13, Helmstaedt & Dixon 1980). If the deformation had been discontinuous, the host pyrite would show two sets of unrelated pressure shadows.

(1) *Steep fold limb*: euhedral pyrites (post-S_1 growth) in a slate with an S_2 crenulation cleavage show 'feathered' fibres with curved face-controlled quartz pressure fringes (Fig. 8i). Using the 'pyrite method' (cf Durney & Ramsay 1973, p. 92, Spencer 1991) the total and incremental strains were calculated from the curvature of partition lines measured relative to the S_2 cleavage (see Gray & Durney 1979, fig. 7 B, 2-eu) (Table 2). Incremental extensions approximated simple shear which is characterized by a constant slope of one radian per unit strain, or $d\phi/de_1 = 5.7°/0.1$ (where ϕ is the orientation of e_1 relative to some fixed reference and e_1 is the principal incremental extension). Total stretches $(1 + e_1)$ ranged from 1.8 to 2.29 (Table 2) with angular discordance between the S_2 cleavage and the total crenulation strain as much as 14°.

(2) *Upright fold limb* with quartz fibre pressure shadows on framboidal pyrite in a slate with crenulated slaty cleavage: long, slender quartz fibres are initially elongated sub-parallel to the S_1 fabric but show a change in orientation through 90° with the last fibre segments parallel to the axial surface direction of F_3 crenulations (Fig. 8j). Using the 'pyrite method' (cf Durney & Ramsay 1973, p. 92, Spencer 1991) the total strains and incremental extensions were calculated from the quartz fibres measured relative to the S_1 cleavage (Table 2). Total stretches $(1 + e_1)$ ranged from 3.0 to 3.06 for the co-axial D_1 deformation increments and 1.31 for co-axial D_2 deformation increments (see Gray & Durney 1979, fig. 13).

Overprinting crenulation cleavages

Zones of mesofolds and crenulation cleavage (Figs. 7d–f) also occur locally outside the polydeformed (slide) zones (Fig. 5). Although the numbers and sequences of these cleavages vary from point to point across the Mount Wellington Fault Zone, crenulation cleavage associations include:

(i) steep crenulation cleavage with an approximate N–S strike (300–020°) deviating up to 70° from the regional fold axial surface trend (approximately 130°). This crenulation cleavage tends to occur along the gently W-dipping upright limbs of the regional folds (Fig. 6e);
(ii) moderately dipping crenulation cleavages on the overturned limbs of the regional asymmetric folds (Fig. 5), or in the gently dipping, intensely foliated parts of the fault zone (Fig. 7d);
(iii) moderately–steeply E-dipping crenulation cleavages locally adjacent to minor faults.

Overprinting crenulation cleavages generally record local variations in the incremental extension direction with respect to pre-existing anisotropies through time (cf Gray & Durney 1979, fig. 17). The local development of crenulation cleavages reflect local kinematics either near faults or within regional and local folds (cf Mosher & Berryhill 1991). Rotation of layering/anisotropy due to movement on curved regional listric faults and/or with progressive folding in a wide zone of simple shear (cf Casey & Huggenberger 1985) can cause multiple crenulation events and resultant cleavages with sufficient strains. This is because the initial layering and the resultant crenulation cleavages rotate in and out of the extension and shortening fields of both the incremental and total strain ellipsoids with high strain during progressive deformation. Strain data in this study indicate principal stretches $(1 + e_1)$ must be >1.3 for a new cleavage to develop; crenulation cleavages are associated with total X/Z strains ranging from 1.7 to 5.3 (Table 2).

What do these tell us about thrust sheet emplacement and post-emplacement deformations? A kinematic model for initiation and development of small-scale

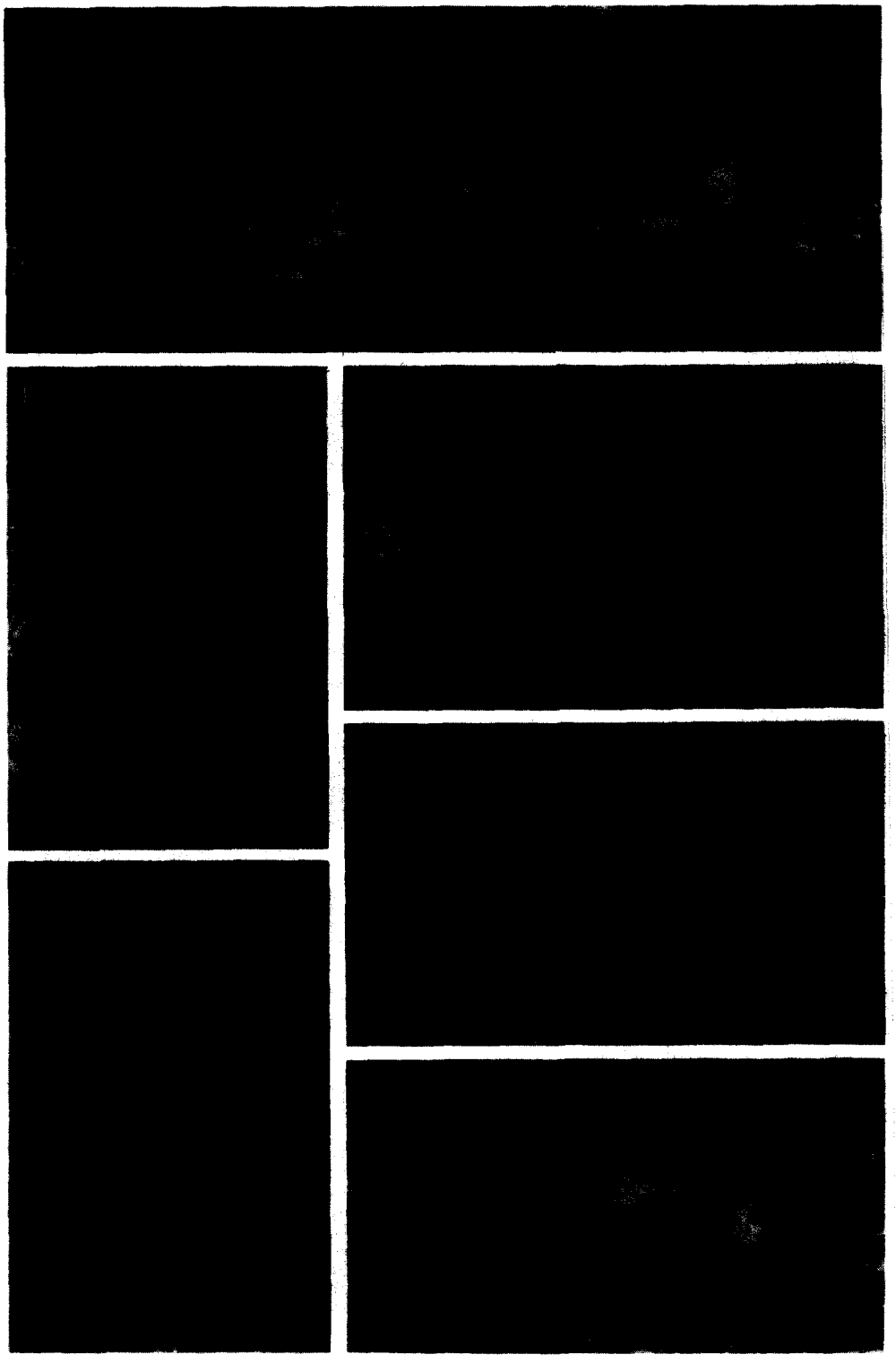

Fig. 7. Structures and structural relationships of the Mount Wellington Fault Zone. (a) Overturned fold showing flat-lying, western limb and overturned, steeply W-dipping, eastern limb (zone 3b). Macalister River, north of Lake Glenmaggie (photo by D. Esser). (b) Tight, upright anticline with weak cleavage in pelitic layers (zone 3a). Road cutting, Thompson Dam road. (c) Deformed cooling columns in weakly cleaved meta-andesite, Licola 'greenstone' window (zone 4) XZ strain is 2.0, where X and Z are the maximum and minimum principal strains respectively. Road cutting on Licola–Jamieson road. Sg: foliation in meta-andesite. Field notebook is 19 cm long. (d) Mesoscopic fold with axial surface crenulation cleavage in transposition layering of the high strain zone above the Jamieson–Licola horse (zone 4). Road cutting, Licola–Jamieson road. Sc: crenulation cleavage. Coin diameter is 28 mm. (e) Transposition layering (S_T) of the high strain zone (zone 4), with asymmetric microfolds in boudinaged and folded quartz veins. Road cutting, Licola–Jamieson road. Sc: crenulation cleavage. Base of photo is 3.2 cm. (f) Discrete crenulation cleavage in deformed sedimentary layering of the high strain zone (zone 4) showing a 'stretched' quartz vein at a low angle to S_T. Road cutting, Licola–Jamieson road. Sc: discrete crenulation cleavage.

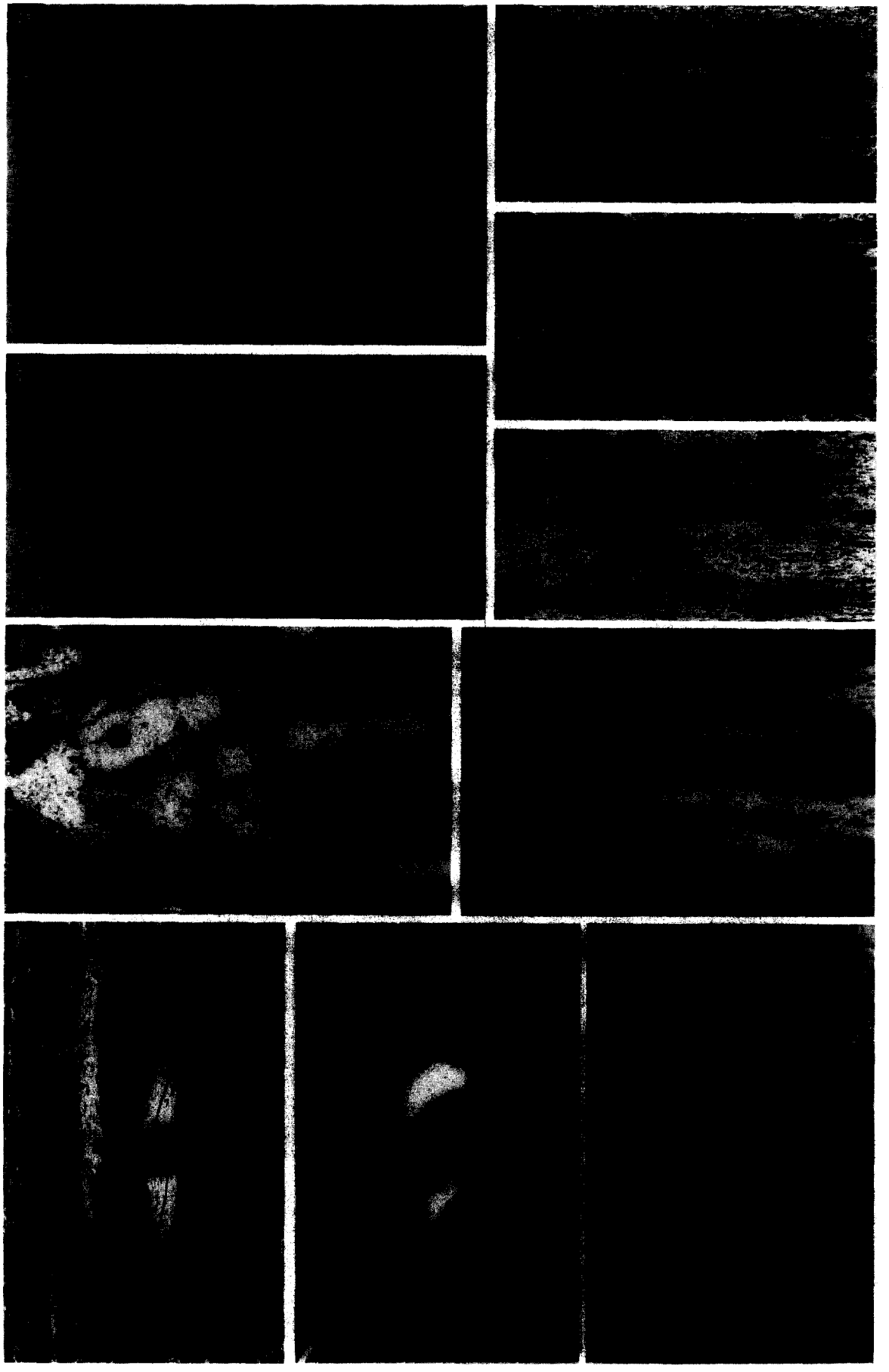

Fig. 8.

crenulation cleavage S_n (see Gray & Durney 1979, fig. 17) requires crenulation of an existing anisotropy (S_{n-1}) once it enters the field of incremental shortening (phase n). S_n will remain stable provided S_{n-1} remains in the field of progressive crenulation shortening and S_n within the field of incremental extension. If neither holds, then a new crenulation S_{n+1} will be initiated. Strain history data (Gray & Durney 1979, Fisher 1990) indicate that initiation of a distinct new cleavage requires an obliquity of at least 45° between the incremental strain axes and the slaty cleavage.

The steeply dipping, approximately strike-parallel, crenulation cleavages on the W-dipping limbs result from sub-horizontal compression within these frontal sheets ('toe shortening') (Fig. 10a), whereas the gently dipping crenulation cleavages require a subvertical compression ('sheet collapse') (Fig. 10b). Continuity in fibre growth in pressure shadows suggest that these cleavages are part of a progressive and continuous deformation. The last crenulation cleavage in all areas is a steep NNE–NE-striking cleavage (see Fig. 5) which reflects a shortening component parallel to the strike of the thrust belt.

Fabric relationships and microstructure of intense cleavage zones

Zones of strongly foliated pelite show transposed bedding, relict isoclinal fold hinges in small quartz veins and markedly attenuated vein limbs (Fig. 7f). Sedimentary layering is almost completely obliterated in places, but rare isoclinal hinges in silstone laminae are preserved (Figs. 8a&b). The cleavage microfabric is dominated by a strong mica preferred orientation (Figs. 8c–e) and thin, dark anastomosing cleavage zones (seams) which truncate isoclinally folded quartz veins (Figs. 7f and 8g). The phyllite microstructure (Fig. 8e) shows relict, isolated, spindle-shaped or ellipsoidal pods of crenulated phyllosilicates, bounded by strongly aligned phyllosilicates parallel to the dominant foliation seen in outcrop. This indicates that this relatively simple foliation seen in outcrop is the product of at least one cycle of near complete transposition (cf Tobisch & Paterson 1988).

Vein segments including relict closures have irregular, sutured contacts indicative of pressure solution (Figs. 7f and 8g). Hinges and limbs of veins show effects of strong dynamic recrystallization with patchy development of small, equant–elongate, polygonal quartz grains and sub-grains. There is no consistent grain elongation or crystallographic preferred orientation. None of the original quartz vein microstructure is preserved. Both the limb and hinge segments of the isoclinally folded veins show considerable numbers of thin (<1 mm) quartz-filled extension fractures which tend to be at high angles to the foliation (Fig. 8f). These micro-veins are generally inclusion-free, clear areas in plane polarized light, but commonly show effects of dynamic recrystallization such as small, strain-free, new grains.

The transposition fabric, therefore, shows a high component of foliation-normal shortening (recorded by the isoclinally folded veins) and foliation parallel extension (recorded by the microscale extension fractures) (Fig. 11).

SIGNIFICANCE

Leading imbricate fan thrust systems are not common in the world's orogenic belts, but are associated with the chevron folded thrust sheets of eastern Australia. The Melbourne Zone of the western Lachlan Fold Belt shows an increase in deformation intensity and metamorphism towards the frontal fault or detachment zone (Table 1 and Fig. 4). Low strains, more open folds and weak cleavage characterize the rear of the belt and imply marked shear displacement on the basal/frontal fault. The amount of internal strain, recorded by regional folding and penetrative fabric development, approximates 32% shortening (Fig. 4). This is low relative to other belts with similar lithologic associations (e.g. ~65% shortening in the Bendigo–Ballarat Zone (Fig. 2), where the deformation is more uniform across the whole belt and individual thrust sheets show marked strain gradients; cf Gray & Willman 1991a). These differences may relate to differences in the initial state (e.g. porosity), depth of burial (i.e. wedge thickness) and in the initial wedge taper at the onset of deformation; an initially high porosity and a higher taper for the sediment wedge would produce a lower internal strain (fold shortening) and little internal imbrication prior to movement (cf Mitra 1994).

In contrast to leading imbricate fan thrust belts, frontal faults in other thrust belts (e.g. Southern Appalachian thrust belt) have low displacement and generally

Fig. 8. Photomicrographs of transposition layering (a–g) and fibrous syntectonic quartz growths in pressure shadows on pyrite (h–j). (a) Isoclinal fold in siltstone layer, showing strong tectonic banding (S_T) sub-parallel to bedding along the limbs. Base of photo is 4.6 cm. (Jamieson–Licola road; DG86-52c.) (b) Hinge of isoclinal fold shown in (a), showing mudstone in the core of fold surrounded by siltstone. Base of photo is 20 mm; S_T is transposition layering. (c) Transposition layering defined by alternating quartz-rich (formerly siltstone) and mica-rich (formerly mudstone) layers. Base of photo is 2.8 mm. (d) Strong mica fabric within mica-rich band is sub-parallel to the banding, but is at a low angle to banding in the quartz-rich (formerly siltstone) layers. Base of photo is 1 mm. (e) Strongly oriented white mica fabric defining the transposition layering within the mica-rich bands. Base of photo is 250 μm. (f) Extension fractures 'h' cutting across the hinge of an isoclinally folded quartz vein. Fractures are at a high angle to the transposition layering (S_T) and are healed by elongate to polygonal quartz grains and oriented phyllosilicates. Base of photo is 1.5 mm. (g) Hinge of isoclinal fold in quartz vein within transposition layering (S_T). Base of photo is 2 mm. (h) Long, slightly curved fibres in strongly cleaved and lineated black slate, Mt Eastern Shale (Jamieson horse; DG84-3); S_1 is slaty cleavage fabric. Base of photo is 200 μm. (i) Pressure shadow with curved partition line approximating 'simple shear' deformation during development of a steep crenulation cleavage (S_c). The buckled quartz vein (white) is sub-parallel to S_1. The sample is from a steep, eastern fold limb position. Base of photo is 500 μm (MU93873). (j) Coarse bladed quartz in pressure fringe, showing continuity of quartz fibre growth between development of the slaty cleavage fabric (S_1) and the crenulation cleavage (S_c). Upright western fold limb position.

Table 2. Summary of total strain data (see Appendix) from the Mount Wellington Fault Zone

Lithology	$1+e_1$	R (XZ)	Structural location	Zone	Map number (Fig. 9)
D_1 deformation					
Black shale	1.4 ($1+e$)	—	Upright fold zone	2a	1
Black slate	2.5	6.3	Upright fold zone	2b	2
Green slate	3.2	10.2	Inclined fold zone	3	3
Green slate	3.1	9.6	Inclined fold zone	3	3
Green slate	3.9	15.2	Inclined fold zone	3	4
Green slate	3.1	9.6	Inclined fold zone	3	5
Black slate	3.2	10.2	Jamieson inlier	4	6
Black slate	4.3	18.4	Jamieson inlier	4	7
Tuffaceous slate	3.0	9.0	Jamieson inlier	4	7
Meta-andesite	—	3.5	Jamieson inlier	4	8
Meta-rhyolite	3.6	12.6	Jamieson inlier	4	9
Vulcanogenic sediment	2.3	5.4	Jamieson inlier	4	10
Meta-andesite	—	2.0	Licola inlier	4	11
D_2 Deformation					
Green slate	1.3	1.7	Inclined fold zone (F_2 crenulations)	3	5
Green slate	1.8	3.3	Inclined fold zone (moderate S_2 cleavage)	3	12
Green slate	2.3	5.3	Inclined fold zone (strong S_2 cleavage)	3	12

low strain. Frontal thrust sheets within these belts also tend to have lower internal strains and limited folding (fault shortening > fold shortening). Most have an imbricate fan geometry, where faults merge with a deeper level décollement. Maximum deformation commonly occurs within root zones in the internal zones to these belts. Root zones are narrow zones where faults merge, show more intense deformation (mylonites), abundance of basement and greater development of horses and duplexes (Boyer & Elliott 1982). No root zones have been located within the Tasmanides of eastern Australia. Questions can be posed as to why this belt is a leading imbricate fan and what this means for thrust mechanics.

Emplacement in many thrust belts is considered the result of successive imbrication of the foot wall with accretion to the hanging wall (Elliott 1976). Combinations of geometrical, kinematic and microstructural evidence presented in this paper (e.g. Figs. 11 and 12) suggest that this is only part of the story for this leading imbricate fan thrust belt. Duplexing is important in the lower part of a two-tiered detachment zone and probably represents foot wall accretion (Fig. 12). The presence of an extensive (0.5–1 km thick) high strain, phyllonite zone with transposition layering above the basal duplex zone suggests, however, that the upper, structurally higher folded zone (zones 1 and 2, Fig. 4) has been transported by confined flow in this phyllonite. Measured strains (Table 2) presumably reflect the overall thickening of the thrust sheet and shortening of the sheet in the transport direction, where ductile yield in the hanging wall is recorded by chevron folding and cleavage development. Whether this can be unequivocally linked to the strong–intense penetrative deformation (transposition layering) at the base of the thrust system is unresolved.

Coupling between the lower duplex zone and the zone of transposition, as suggested by the incorporation of Cambrian metavolcanic slices into the phyllonite zone, would however require the transport of the duplex zone 'en masse' up the lowest and last-formed imbricate thrust fault (Dahlstrom 1969, p. 369). This would explain the development of the leading edge imbricate stack (Dahlstrom 1969) or leading imbricate fan (Boyer & Elliott 1982) geometry, and perhaps indicate that the strain gradients are a relict of the earlier history rather than related to the present geometry. Assemblages defining either the foliated margins and/or shear zones within these Cambrian slices (chlorite–actinolite assemblages) indicate temperatures of 350–400°C and pressures of 2–4 kb during foliation development and presumably horse formation, indicating that the detachment was initiated at a depth of 7–12 km.

Some of the differences in the toe region or at the leading edge with respect to other classic thrust belts may also be due to complications caused by the convergence of this younger, E-directed thrust belt (Melbourne Zone) with an earlier, W-directed system (Tabberabbera Zone) (see Fig. 2). Interpretation (Fig. 2) has the younger thrust system truncating the older, although the boundary between the two belts is probably along the Dolodrook fault system enclosing Alpine ultramafics (see Dolodrook 'greenstones', Fig. 5).

What does the Mount Wellington Fault Zone have to tell us about thrusting processes? This fault zone shows strongly heterogeneous deformation with strong to intensely foliated transposition zones enclosing fault-bounded slices (horses?) of different lithologies and domains where relict-folded, sedimentary layering is preserved. Strain is variable, but shows a marked increase into the fault zone (see Fig. 4c, Table 2 and Appendix). Development of asymmetric regional folds

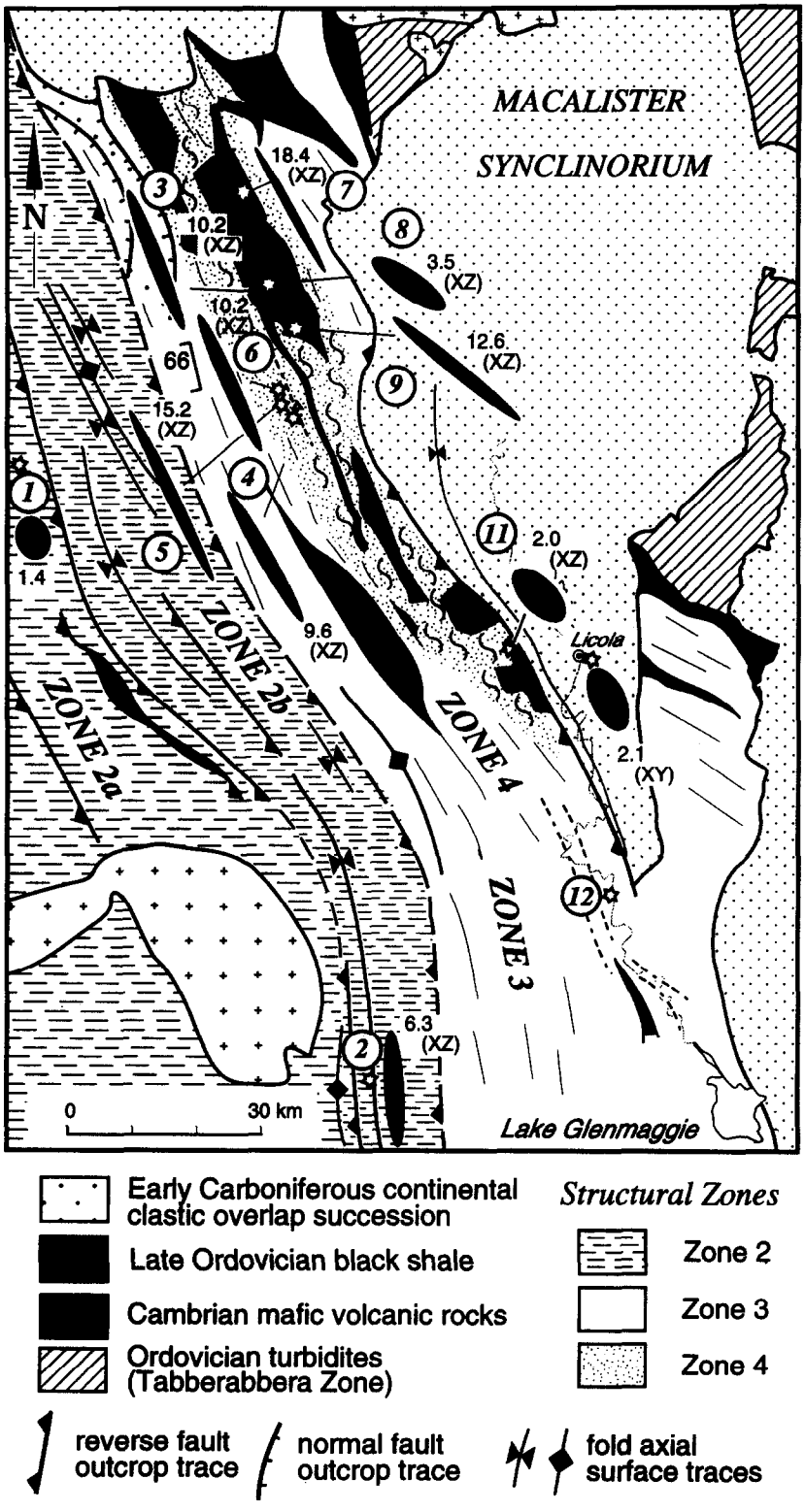

Fig. 9. Strain map, structural zones and geological relationships of the Mount Wellington Fault Zone. Locations of strain determinations (see Appendix) shown by star with circled locality numbers corresponding to those listed in Table 2. Total strain magnitudes are shown by black ellipses with designations as either X/Z or X/Y strains.

and the incorporation of fault-bounded slices into a zone of transposition layering all have consequences for initiation of, and motion within, the detachment zone.

Significance of asymmetric folds

Although the record of rotational deformation is limited, the transition from upright to overturned folds is an integral part of the strain gradient into the fault zone (see Table 1 and Fig. 3) and must reflect an increase in shear strain towards the basal detachment fault (e.g. Sanderson 1979, 1982, Gibson & Gray 1985, Gray & Willman 1991). Asymmetric fold development has been related to a 'rolling hinge' model involving alternating fixed (pinned) and rotating limbs (Beutner & Diegle 1985) and to folding of layers at low angles to shear zone boundaries (Casey & Huggenberger 1985).

Fibres in pressures shadows from the inclined fold

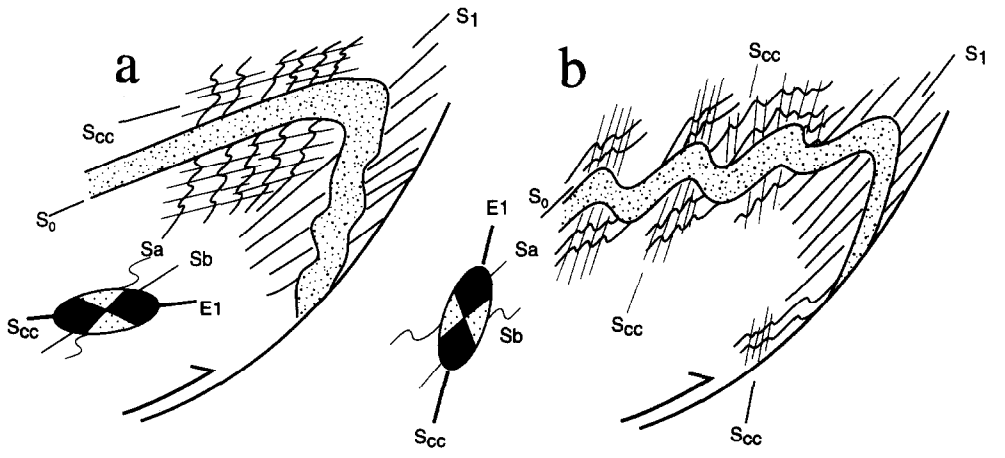

Fig. 10. Relationships between overprinting crenulation cleavages and regional folds within zones 3 and 4. (a) Gently dipping crenulation cleavage in S_1 on upright limb with mesofolds in S_0 on the overturned limb. (b) Steep crenulation cleavage in S_1 and associated mesofolds in S_0 on upright limb. Strain ellipse shows shortening and extension fields for the crenulation deformation event; E_1 is the direction of maximum principal stretch for the respective crenulation deformation events.

zone (zone 3) in the Mount Wellington Fault Zone are relatively straight and sub-parallel to the S_1 fabric. The observed straight fibres on upright limbs of asymmetric regional folds requires a co-axial deformation sequence (Fig. 12a), whereas weakly curved fibres on overturned limbs suggest some rotation accompanied fold/cleavage development (Fig. 12d). These folds may have formed by pinning of the upright, gently W-dipping, western limbs with rotation of the eastern limbs from a steep easterly dip to an overturned, steep westerly dip, due largely to a component of shear induced vorticity (SHIV: Lister & Williams 1983). The low fibre curvature indicates, however, that plane strain flattening still dominates foliation development along these fold limbs (Fig. 12d). Limb rotation causing fold asymmetry into the fault zone was, therefore, not necessarily accompanied by penetrative strain. This part of the deformation must have been quite heterogeneous and is reflected by sporadic development of a simple, shear-related crenulation cleavage on the overturned limb (Fig. 12c). This association suggests that increased shear strain gradients must have occurred along the steep–overturned limbs of these folds late in the fold development. If layer rotation had been interspersed with flattening increments as the asymmetric folds and cleavage developed, then the pressure shadows would show the opposite curvature to that observed (see Beutner & Diegle 1985, fig. 8: compare b & c).

Fibre geometries typical of those found on the overturned fold limbs of the asymmetric regional folds (see position D, Fig. 11) are found in pressure shadows on framboidal pyrite within the fault-bounded slices of Upper Ordovician slate. These also generally show W-vergent, homoclinally dipping bedding and slaty cleavage, further indicating that they are derived from the steeper E-dipping limbs of the asymmetric regional folds (Figs. 6f & g). This suggests that all or much of the folding of the thrust sheet proper occurred prior to significant movement along the basal zone and, therefore, prior to the movement which changed the geometry of the belt to that of a leading imbricate fan.

Transposition: implications for thrust motion

The basal phyllonite zone consists of strongly foliated phyllite with foliation-parallel compositional banding representing transposed bedding (Fig. 11b). The presence of dismembered isoclinally folded quartz veins (Figs. 8f & g) and isoclinal hinges in thin sandstone/siltstone layers (Figs. 8a&b) suggests that the foliation is the result of a very large ductile strain within a progressively deforming shear zone undergoing cyclic transposition (cf. Tobisch & Paterson 1988, Mawer & Williams 1991).

Such transposition 'cycling' involves obliteration of crenulations to produce a 'continuous' cleavage with slaty–phyllitic morphology. Re-crenulation of this continuous cleavage and repetition of the process will occur at high strains and large shear displacement in the phyllonite zone. The developing foliation approximates a steady-state feature continually reconstituted by microscale transposition and recrystallization. Individual micas either undergo kinking and dynamic recrystallization (e.g. Mawer & Williams 1991, figs. 17 and 18) or are crenulated within the early foliation with subsequent overprinting by a strong, axial, surface-parallel mica fabric to produce a new schistosity or continuous cleavage (e.g. Tobisch & Paterson 1988). Transitions from an early continuous cleavage (S_c) to crenulation cleavage (S_{cr}) to a new continuous cleavage/

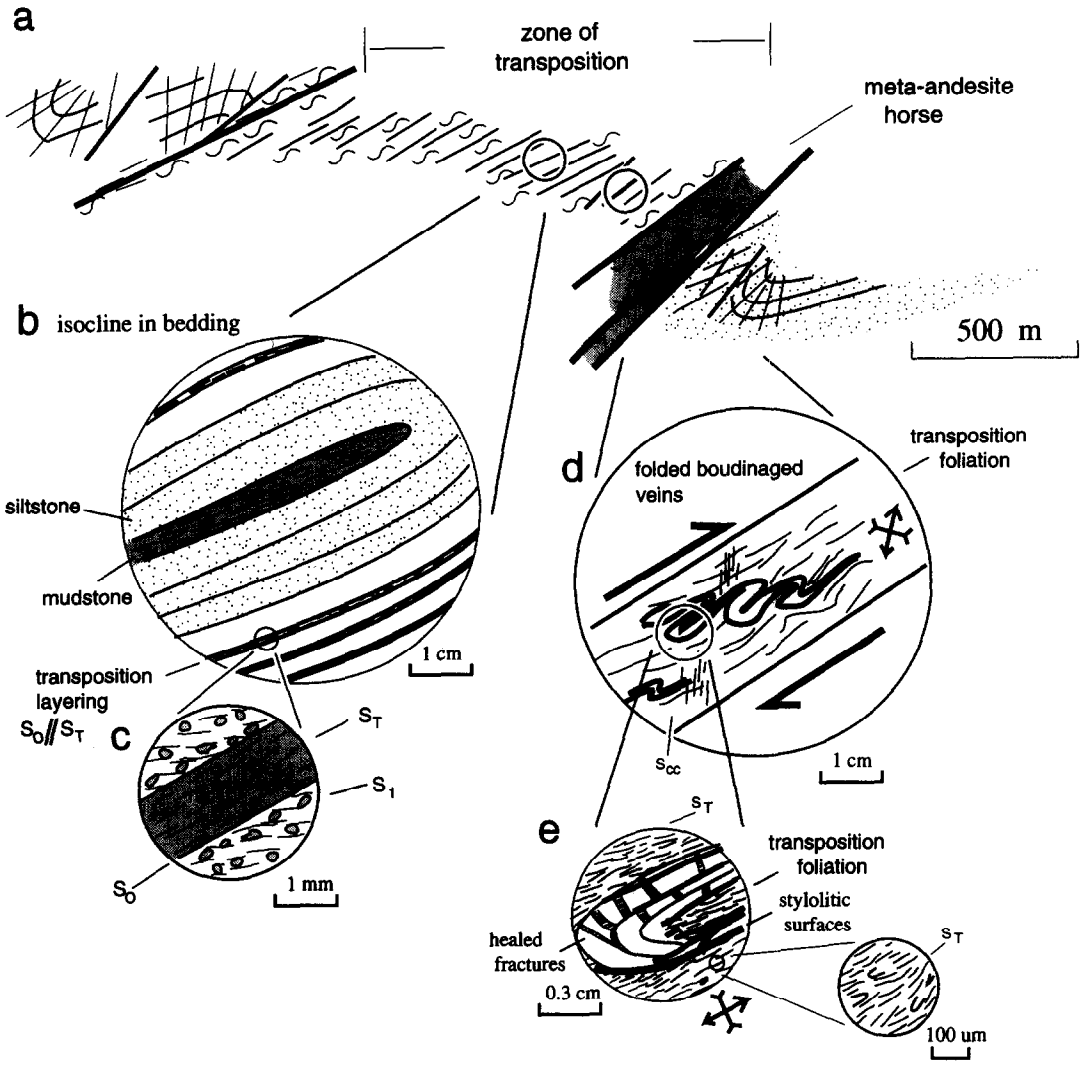

Fig. 11. Deformation kinematics for zone of transposition cycling. (a) Structural profile showing zone of transposition layering/foliation typical of zone 4 (for location see section line 'f' on Fig. 5). (b) Isocline in laminated siltstone and mudstone from zone of transposition layering where bedding (S_0) and transposition foliation (S_T) are sub-parallel. (c) Enlargement showing S_0/S_T in pelite and cleavage (S_1) and bedding at very low angle (<5°). (d) Structural relations within transposition foliation showing folded boudinaged veins and overprinting crenulation cleavage (S_{cc}). (e) Enlargement of hinge in buckled quartz vein showing healed microfractures at high angles to S_T and stylolitic surfaces sub-parallel to S_T.

transposition fabric (S_T) are all potentially part of a continuum in progressively evolving shear zones within pelitic rocks (cf Tobisch & Paterson 1988). The strong mica fabric (Figs. 8d & e) and the rare occurrence of foliation 'fish' (e.g. Hanmer & Passchier 1991), containing relict isoclinal hooks and crenulations in earlier mica fabrics, suggest continuous mica recrystallization and growth of new mica. The continuous reconstitution of mica in the phyllonite as such produces a strain softening fabric where the large ductile strains are recorded by isoclinally folded and dismembered quartz veins.

CONCLUSIONS

Detachment zones associated with leading imbricate-fan fold and thrust belts are zones of stronger deformation showing marked strain gradients of the regional deformation into their zones. In the Lachlan Fold Belt of eastern Australia there is a complete transition from upper level, non-to weakly cleaved rocks associated with open folds into lower level, strongly cleaved, close–tight overturned folds cut by numerous brittle faults, into the basal shear zone (detachment zone) defined by intensely foliated phyllonitic rocks with isoclinally folded quartz veins and sedimentary layering, overlying a duplex zone in Cambrian metavolcanics (Fig. 13). Deformation occurs over a wide zone and is markedly heterogeneous with relict fold structures truncated by brittle faults separated by intensely foliated zones which enclose tapered, pod-shaped horses of structurally lower rocks derived from lower level detachments.

(1) Leading imbricate-fan thrust belts are a consequence of transport of a detachment zone (phyllonite zone plus basal duplex zone in the case of the Mount Wellington Fault Zone) up the lowest and last formed imbricate fault.

(2) Deformation either occurred within fault-bounded polydeformed zones (slides) or within shear zones characterized by intense transposition fabrics in

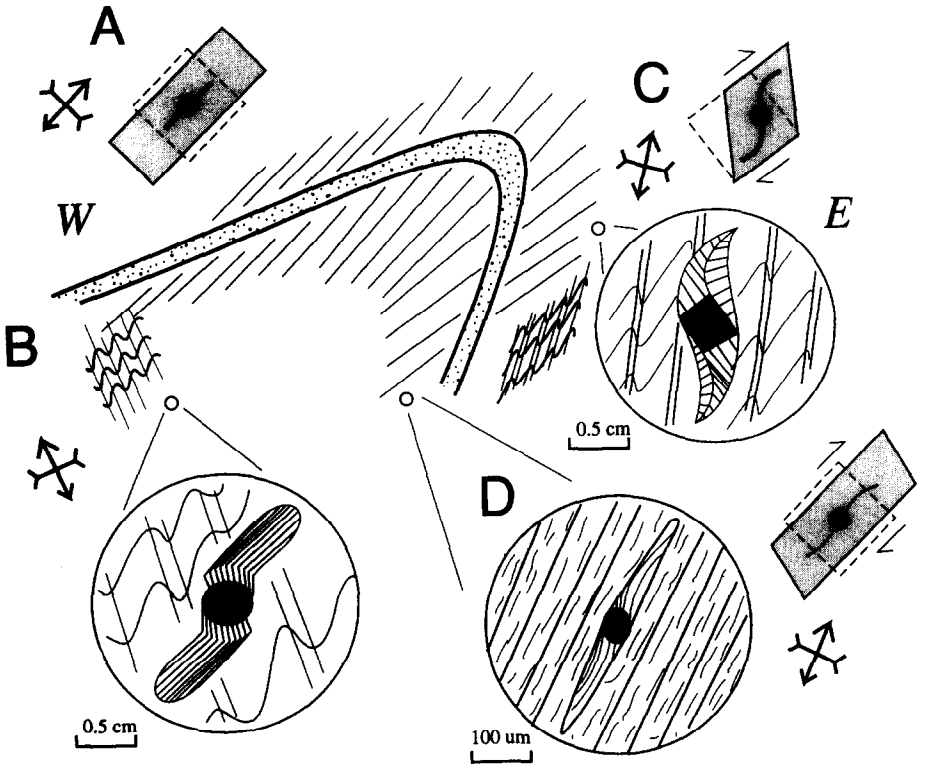

Fig. 12. Deformation kinematics for overturned folds (zones 3 and 4). Deformation scenarios with instantaneous stretching and shortening axes shown for different structural positions. (a) Plane strain flattening with development of axial surface cleavage (common on upright limb and hinge of regional F_1 folds). (b) Continuous deformation on upright limb with development of a strike-parallel, moderately–steeply dipping crenulation cleavage. Pressure shadows indicate a continuous, progressive deformation. (c) Progressive simple shear along S_1 with development of a crenulation cleavage (overturned, structurally lower limbs of regional F_1 folds). (d) Plane strain flattening with minor rotation component (overturned, structurally lower limbs of regional F_1 folds).

phyllonites towards the base of the composite thrust sheet. The polydeformed zones represent more intense regional deformation, where locally higher strain rates facilitated polydeformation with development of overprinting crenulation cleavages, local reorientation and refolding of F_1 fold closures and localized mesoscale fold interference patterns.

(3) Phyllonites define a region of transposition cycling and probably represent localized strain softening at the base of the composite thrust sheet.

(4) Fault-bounded slices of Cambrian volcanics represent detached segments from a lower level duplex zone which originated at 7–12 km depth (based on metamorphic mineral assemblages within the horses).

(5) The larger, fault-bounded slices have largely behaved as rigid blocks during emplacement to present

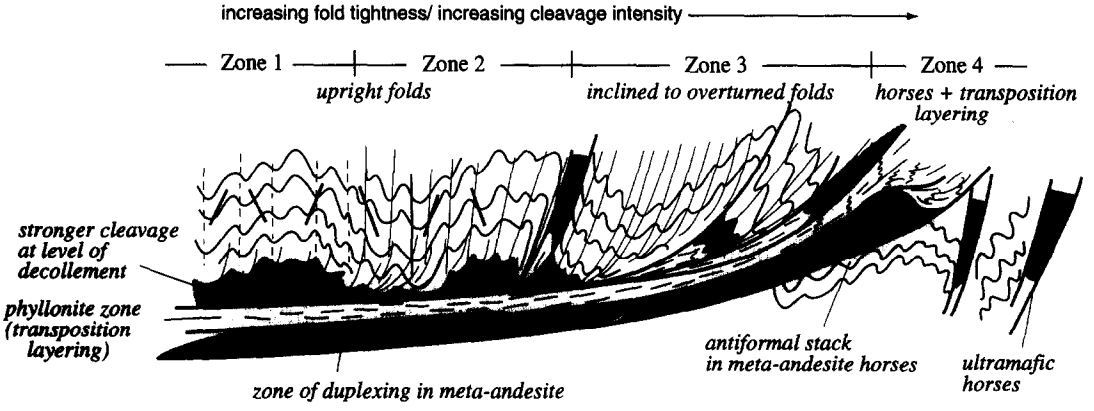

Fig. 13. Schematic structural profile for leading imbricate-fan thrust belt developed within 'oceanic' sequence incorporating turbidites (interbedded sandstone and mudstone sequence) overlying 'oceanic crust' (meta-basalt and meta-andesite). Wedge shortening and emplacement incorporates a three-tiered deformation zone with an upper level tier of fold shortening overlying lower tiers of transposition cycling (0.5–1 km thick mylonite zone) and duplexing (within ~5 km thick mafic igneous rocks of oceanic affinity); black = Cambrian mafic–ultramafic rocks; grey = Upper Ordovician black shale/slate.

structural levels. Margins of these tapered, elongate slivers are strongly foliated and structurally concordant with the foliations in the surrounding rocks.

(6) Overprinting crenulation cleavages (polydeformation) reflect the thrust sheet emplacement history: combinations of *thrust loading* (generating sub-horizontal–moderately dipping S_2 crenulation cleavages along overturned fold limbs), *toe compression* (generating upright mesofolds and steeply dipping S_3 crenulation cleavages on upright limbs and locally overprinting flat S_2 cleavages on overturned limbs), and localized *strike-parallel compression* to give sub-vertical strike-perpendicular crenulation cleavages.

Acknowledgements—The research was supported in part by Australian Research Council Grants E8315666 and E8315675 and an ARC Monash Small Grant in 1994. The work has benefited from discussions with Chris Fergusson, Nick Woodward, Chris Wilson, Robert Gregory and Ray Cas. The study would not have been possible without the regional mapping of Fons VandenBerg (Victorian Geological Survey) and structural mapping by Monash University Honours students (Nigel Murphy, David Esser, Martin Bonwick, Greg Robinson and Steve Andrews) and La Trobe University Honours students (Mark Hendrickx and Jonathan Kelly). DRG acknowledges (1) discussions with Fons VandenBerg, Clive Willman and Marc Hendickx about recent detailed mapping by the Victorian Geological Survey in the Mount Wellington Fault Zone; (2) Marc Hendrickx for access to his thin sections from the Jamieson area; (3) Robin Offler for access to unpublished illite crystallinity data. Support (teaching relief in 1994) by the Australian Geodynamics Crustal Research Centre (AGCRC) has enabled completion of the research and manuscript. Comments by Tim Little, Richard Norris and an anonymous reviewer significantly improved the manuscript.

REFERENCES

Beutner, E. C. & Diegel, F. A. 1985. Determination of fold kinematics from syntectonic fibers in pressure shadows, Martinsburg Slate, New Jersey. *Am. J. Sci.* **285**, 16–50.

Boyer, S. E. & Elliott D. 1982. Thrust Systems. *Bull. Am. Ass. Petrol Geol.* **66**, 1196–1230.

Casey, M. & Huggenberger, P. 1985. Numerical modelling of finite amplitude similar folds developed under general deformation histories. *J. Struct. Geol.* **7**, 103–114.

Crawford, A. J. 1988. Cambrian. In: *Geology of Victoria* (second edition) (edited by Douglas, J. G. & Ferguson, J. A.). *Geol. Soc. Aust. Victorian Div.*, Melbourne, pp. 37–62.

Dahlstrom, C. D. A. 1969. Balanced cross-sections. *Can. J. Earth Sci.* **6**, 743–757.

Durney, D. W. & Ramsay, J. G. 1973. Incremental strains measured by syntectonic crystal growths. In: *Gravity and Tectonics* (edited by De Jong, K. A. & Scholten, R.). Wiley, New York, pp. 67–96.

Elliott, D. 1976. The energy balance and deformation mechanisms of thrust-sheets. *Phil. Trans. R. Soc. Lond.* **A283**, 289–312.

Fergusson, C. L. & Coney, P. J. 1992. Convergence and intraplate deformation in the Lachlan Fold Belt of southeastern Australia. *Tectonophysics* **214**, 417–439.

Fergusson, C. L., Gray, D. R. & Cas, R. A. F. 1986, Overthrust terranes in the Lachlan Fold Belt, southeastern Australia. *Geology* **14**, 519–522.

Fisher, D. M. 1990. Orientation history and rheology in slates, Kodiak and Afognak Islands, Alaska. *J. Struct. Geol.* **12**, 483–498.

Fischer, M. & Coward, M. 1982. Strains and folds within thrust-sheets: an analysis of the Heilam sheet, northwest Scotland. *Tectonophysics* **88**, 291–312.

Geiser, P. A. 1988. Mechanisms of thrust propagation: some examples and implications for the analysis of overthrust terranes. *J. Struct. Geol.* **10**, 829–845.

Gibson, G., Wesson, V. & Cuthbertson, R. 1981. Seismicity of Victoria to 1980. *J. geol. Soc. Aust.* **28**, 341–356.

Gibson, R. G. & Gray, D. R. 1985. Ductile-to-brittle transition in shear during thrust-sheet emplacement, southern Appalachian thrust belt. *J. Struct. Geol.* **7**, 513–525.

Glen, R. A. 1992. Thrust, extensional and strike-slip tectonics in an evolving Palaeozoic Orogen of southeastern Australia. *Tectonophysics* **214**, 341–380.

Gray, D. R. 1988. Structure and Tectonics, In: *Geology Of Victoria* (second edition) (edited by Douglas, J. G. & Ferguson, J. A.). *Geol. Soc. Aust. Victorian. Div.*, Melbourne, pp. 1–36.

Gray, D. R. & Durney, D. W. 1979. Investigations on the mechanical significance of crenulation cleavage. *Tectonophysics* **58**, 35–79.

Gray, D. R. & Willman, C. E. 1991a. Thrust-related strain gradients and thrusting mechanisms in a chevron-folded sequence, southeastern Australia. *J. Struct. Geol.* **13**, 691–710.

Gray, D. R. & Willman, C. E. 1991b. Deformation in the Ballarat Slate Belt, Central Victoria and implications for the crustal structure across SE Australia. *Aust. J. Earth Sci.* **38**, 171–201.

Gray, D. R., Wilson, C. J. L. & Barton, T. J. 1991. Intracrustal detachments and implications for crustal evolution within the Lachlan Fold Belt, southeastern Australia. *Geology* **19**, 574–577.

Hanmer, S. & Passchier, C. W. 1991. Shear sense indicators: a review. *Geol. Surv. Pap. Can.* 90–117.

Harris, W. J. & Thomas, D. E. 1954. Notes on the geology of the Wellington–Macalister Area. *Min. Geol. J. Vic.* **5**, 34–49.

Helmstaedt, H. J. & Dixon, J. 1980. Superposed crenulation cleavages resulting from progressive deformation. *Tectonophysics* **66**, 115–126.

Hendrickx, M. 1993. The Geology of the Jamieson Inlier, central eastern Victoria. unpublished B.Sc. (Hons) Thesis, LaTrobe University, Melbourne.

Lister, G. S. & Williams, P. F. 1983. The partitioning of deformation in flowing rock masses. *Tectonophysics* **92**, 1–33.

Mawer, C. K. & Williams, P. F. 1991. Progressive folding and foliation development in a sheared, coticule-bearing phyllite. *J. Struct. Geol.* **13**, 539–555.

Mitra, G. 1994. Strain variation in thrust sheets across the Sevier fold-and-thrust belt (Idaho–Utah–Wyoming): implications for section restoration and wedge taper evolution. *J. Struct. Geol.* **16**, 585–602.

Mosher, S. & Berryhill, A. W. 1991. Structural analysis of progressive deformation within complex transcurrent shear zone systems: southern Narragansett Basin, Rhode Island. *J. Struct. Geol.* **13**, 557–578.

Murphy, N. C. & Gray, D. R. 1992. East-directed overthrusting in the Melbourne Zone, Lachlan Fold Belt. *Aust. J. Earth Sci.* **39**, 37–53.

Odonne, F. & Vialon, P. 1987. Hinge migration as a mechanism of superimposed folding. *J. Struct. Geol.* **9**, 835–844.

Ramsay, J. G. & Huber, M. I. 1983. *The Techniques of Modern Structural Geology. Volume* 1: *Strain Analysis*. Academic Press, New York.

Sanderson, D. J. 1977. The analysis of finite strain using lines with an initial random orientation. *Tectonophysics* **43**, 199–211.

Sanderson, D. J. 1979. The transition from upright to recumbent folding in the Variscan fold belt of southwest England: a model based on the kinematics of simple shear. *J. Struct. Geol.* **1**, 171–180.

Sanderson, D. J. 1982. Models of strain variation in nappes and thrust sheets: a review. *Tectonophysics* **88**, 201–233.

Spencer, S. 1991. The use of syntectonic fibres to determine strain estimates and deformation paths: an appraisal. *Tectonophysics* **194**, 13–34.

Tobisch, O. T. & Paterson, S. R. 1988. Analysis and interpretation of composite foliations in areas of progressive deformation. *J. Struct. Geol.* **10**, 745–754.

VandenBerg, A. H. M. 1977. *Warburton* 1:250,000 *Geological Map*. Geological Survey of Victoria, Melbourne.

VandenBerg, A. H. M. 1978. The Tasman Fold Belt System. *Tectonophysics* **48**, 267–279.

VandenBerg, A. H. M. 1988. Silurian–Middle Devonian, In: *Geology Of Victoria* (second edition) (edited by Douglas, J. G. & Ferguson, J. A.). *Geol. Soc. Aust. Victorian Div.*, Melbourne, pp. 103–146.

APPENDIX

Total strain data for the Mount Wellington Fault Zone

Sample locality	Strain marker	l_0	l_1	Elongation e_1	Stretch $1+e_1$	Strain ratio (R)	Structural element	Lithology
Enochs Point GR. 206540	Graptolites* in S_0 $S_0 \wedge S_1$:	—	—	—	1.4 (1+ e in S_0)		S_0	Black shale (Upper Ordovician)
Walhalla GR. 511914	Pressure shadow†	6	15	1.5			S_1	Dark grey slate (Devonian)
		3	9	2.0				
		3.2	7	1.2				
		5.5	22	1.5				
		6	16	1.6				
				$x = 1.6$	2.6	6.8*		
Jamieson South Track GR. 459631	Pressure shadow	6	21	2.5	3.5	12.6*	S_1	Altered rhyolite lava (Cambrian?)
Jamieson–Mt Sunday road GR. 423652	Pressure shadow	3.8	10	1.63			S_1	Black slate (Upper Ordovician)
		4.0	13	2.25				
		2.8	10	2.5				
		2.0	7	2.5				
		2.9	9	2.1				
				$x = 2.2$	3.2	10.2*		
Jamieson–Mt Sunday road GR. 425726	Pressure shadow	9.0	22	1.4			S_1	Tuffaceous slate (Upper Ordovocian)
		3.0	9	2.0				
		5.0	12	1.4				
		1.5	6	3.0				
				$x = 2.0$	3.0	9.0*		
Jamieson–Mt Sunday road GR. 425726	Pressure shadow	3.5	17	3.9			S_1	Black slate (Upper Ordovician)
		3.0	10	2.3				
		2.0	11	4.5				
		2.6	9.0	2.5				
				$x = 3.3$	4.3	18.4*		
Jamieson–Mt Sunday road GR. 432636	Pressure shadow	3	7	1.33	2.33	5.4*	S_3	Vulcanogenic sediment (Cambrian?)
Jamieson–Mt Sunday road GR. 443665	Flattened cooling columns	—	—	—	—	3.5	S_1	Meta-andesite (Cambrian?)
Jamieson–Licola road GR. 621391	Flattened cooling columns	—	—	—	—	2.0	S_1	Meta-andesite (Cambrian?)
Snake Edwards Divide GR. 417600	Pressure shadows	4	15	2.9			S_1	Olive-green slate (Silurian
		4	16	3.0				
		4	15	2.9				
		4	16	3.0				
				$x = 2.9$	3.9	15.2		
Snake Edwards Divide GR. 414599	Pressure shadows	2.5	8	2.2			S_1	Olive-green slate (Silurian?)
		6.0	17	1.8				
		3.5	12	2.4				
				$x = 2.1$	3.1	9.6		
Mt Skene GR. 447576	Pressure shadow	16	49	2.1	3.1	9.6*	S_1	Olive-green slate (Silurian?)
		7	21	2.0	3.0	9.0*		
		16	21	0.3	1.3	1.7*	S_2	
Mt Skene GR. 449572	Pressure shadow	6.5	18	1.8			S_1	Olive-green slate (Silurian?)
		3.5	10	1.9				
		4.0	14	2.5				
		7.0	20	1.9				
		3.0	10	2.3				
		2.6	9	2.5				
				$x = 2.2$	3.2	10.2*		
Macalister River GR. 711142	Curved anti-axial quartz fibres in pressure shadows	—	—	—	1.8	3.3	Moderate S_2	Olive-green slate
		—	—	—	2.3	5.3	Strong S_2	(Silurian?)
		—	—	—	1.8	3.2	Moderate S_2	
		—	—	—	1.5	2.3	Weak S_2	
Jamieson–Mt Skene road GR. 353671	Reduction spots					1.4 (XY) $n = 3$	Weak S_1	Maroon mudstone/ siltstone (Early Carboniferous)
Licola GR. 669351	Reduction spots					2.1 (XY) $n = 9$	Weak S_1	Maroon mudstone/ siltstone (Early Carboniferous)

Note: l_0 and l_1 are the undeformed length (pyrite radius) and deformed length (fibre length), respectively (determined from pressure shadows); elongation $e_1 = (l_1 - l_0)/l_0$; strain ratio R is calculated assuming a plane strain, constant volume deformation [i.e. $1 + e_3 = 1/(1 + e_1)$].

*Graptolites: strains were calculated in the plane of bedding using thecal angles and stipe orientation (see Ramsay & Huber 1983, pp. 136–140).

†Pressure shadows: strains were calculated using the Pyrite method of Durney & Ramsay (1973) (see also Spencer 1991).